position for the water molecules is one in which there is minimal interference in the interaction between the ions. The close approach of Mg^{2+} to the phosphorus atom is not markedly altered by two waters, although these waters optimize their positions to allow maximum interionic interactions. The steepness of the potential curve in Figure 3 is consistent with ion-pair formation in solution, although these calculations with only two water molecules cannot definitively argue for site binding of Mg^{2+} in solution. However, recent experimental evidence does suggest that Mg^{2+} directly site binds to the phosphate groups of DNA in solution.[20]

Conclusions

Several inferences regarding the possibility of the formation of ion pairs between phosphate and the small cations present in the very high concentrations at nucleic acid surfaces can be made. For the monovalent cations, NH_4^+ and Na^+, similar minima are found for the four molecule potential surface involving phosphate and two water molecules. These minima are distinctly different from the minima that occur with no water present. The effect of the water does not appear to be to solvate the optimal ion pair. Rather the water becomes an integral part of the complex, increasing the anion–cation distance but not disrupting the interaction completely. It seems clear from these calculations that neither NH_4^+ nor Na^+ would form a close contact ion pair with phosphate groups of the nucleic acid backbone. From the shape of the very flat potential (Figure 2) for the interaction of Na^+ with $H_2PO_4^-$ in the presence of two water molecules, it may be concluded that Na^+ would not even form a static hydrated complex of the type indicated by complex XV. Instead, the association of Na^+ with nucleic acids is expected to be completely as mobile ions moving in the highly electrostatic potential surrounding the polyanion.

The binding of Mg^{2+} is much stronger than that of the monovalent cations. The steepness of the potential shown in Figure 3 clearly shows that unlike the monovalent cations, Mg^{2+} cannot be displaced from its site-bound position by the addition of two water molecules. This is an indication that Mg^{2+} might interact by direct site binding, although calculations with only two water molecules are not sufficient to allow definitive statements in this regard.

Acknowledgment. This work was supported by Grant R01-GM29079 from the National Institute of General Medical Sciences. Additional generous support from the Sundstrand Corporation is gratefully acknowledged. We thank Dr. Gilda Loew for helpful discussions on various aspects of this problem.

(20) Taboury, J. A.; Bourtayre, P.; Ligier, J.; Taillandier, E. *Nucleic Acids Res.* **1984**, *12*, 4247-4258.

Cleft Formation upon Polymerization of Surfactant Vesicles

Faruk Nome,[1] Wayne Reed, Mario Politi, Pietro Tundo,[2] and Janos H. Fendler*

Contribution from the Department of Chemistry and Institute of Colloid and Surface Science, Clarkson University, Potsdam, New York 13676. *Received June 1, 1984*

Abstract: Morphological consequences of the photopolymerization of vesicles prepared from $(C_{18}H_{37})_2N^+(CH_3)$-$CH_2C_6H_4$-*p*-$CH{=}CH_2,Cl^-$, **1**, have been investigated by using 8-hydroxy-1,3,6-pyrenetrisulfonate (POH) as a reporter group. Static and dynamic laser light scattering established the hydrodynamic radius and the molecular weight of **1** vesicles to be 425 ± 25 Å and 2.3×10^7. Neither of these values changed upon polymerization. POH was shown to bind appreciably to **1** vesicles. Excitation of POH, following immediately its addition to nonpolymerized **1** vesicles, resulted in fluorescence emission with maxima at 440 and 520 nm. Incubation led to time-dependent changes of this spectra. Increasing incubation time of POH containing nonpolymerized **1** vesicles resulted in the gradual disappearance of the emission band at 520 nm and in the concomitant increase of the emission band at 440 nm. Fluorescence spectra of POH did not show any time-dependent changes following its addition to polymerized **1** vesicles. These results were interpreted in terms of the gradual penetration of POH into nonpolymerized **1** vesicles and in terms of long-term stabilization of POH in the clefts formed on the vesicle surface upon pulling the surfactant head groups together by photopolymerization. Differences between nonpolymerized and polymerized vesicles also manifested in the excited state protonation equilibria

$$(POH)^* \underset{k_{on}^*}{\overset{k_{off}^*}{\rightleftharpoons}} (PO^-)^* + H^+$$

A k_{off}^* value of 4.3×10^9 s^{-1} was obtained in nonpolymerized vesicles immediately after the POH injection. Following a day of incubation no excited-state proton ejection could be observed in nonpolymerized **1** vesicles. Consequently, a k_{off}^* value of 6.1×10^9 s^{-1} was observed in nonpolymerized vesicles both immediately and 1 day subsequent to the addition of POH to polymerized **1** vesicles. Similar behavior has been observed for the steady-state (P) and nanosecond time-resolved polarizations, τ_R values, of POH, as well as that for the ground state PO^- reprotonation (governed by k_{on}) in nonpolymerized and polymerized **1** vesicles. In nonpolymerized **1** vesicles, P values increased (from 0.12 to 0.19), τ_R was determined to be ≥50 ns, and k_{on} values (4×10^8 M^{-1} s^{-1}) became unobservable after a day of incubation. In polymerized **1** vesicles, P values of 0.08, τ_R values of 4 ns, and k_{on} values of 8×10^8 M^{-1} s^{-1} remained unaffected by incubation.

The ever increasing utilization of organized surfactant aggregates in reactivity control, drug delivery, and photosensitized water splitting have necessitated the development of new systems.[3,4] Polymerized surfactant vesicles have become highly popular within a remarkably short time since polymerization has provided an unprecedented degree of stability and permeability control as well as opened the door to domain-controlled substrate release.[5-17]

(1) Permanent Address: Depto. de Quimica, Universidade Federal de Santa Catarina, 88000—Florianopolis, Santa Catarina, Brazil.
(2) Permanent Address: Istituto Di Chimica Organica, Della Universita de Torino, 10125 Torino, Via Bidone 36, Italy.

(3) Fendler, J. H. "Membrane Mimetic Chemistry"; Wiley-Interscience: New York, 1982.
(4) Fendler, J. H. *Chem. Eng. News* **1984**, *Jan. 2*, *62*, 25-38.

0002-7863/84/1506-8086$01.50/0

As part of our ongoing program we have recently elucidated the kinetics and mechanisms of surfactant vesicle photopolymerization. Photolysis of vesicles prepared from surfactants containing styrene moities in their head groups have been shown to result in intravesicular surface polymerization with an average chain length of 20.[16] This polymerization resulted in pulling some of the aromatic rings together, thereby creating clefts on the vesicle surface.[18] Attention in the present work is focussed on obtaining a morphological insight on cleft formation upon the photopolymerization of vesicles prepared from $(C_{18}H_{37})_2N^+(CH_3)$-$CH_2C_6H_4$-*p*-$CH{=}CH_2, Cl^-$ (**1**). Advantage was taken of 8-hydroxy-1,3,6-pyrenetrisulfonate, pyranine (POH) as a sensitive

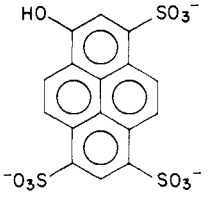

POH

probe to report its environmental changes in terms of steady-state and time-resolved fluorescence spectra and anisotropy as well as in terms of its ground- and excited-state protonation equilibria.[19-24]

Experimental Section

$(C_{18}H_{37})_2N^+(CH_3)CH_2C_6H_4$-*p*-$CH{=}CH_2, Cl^-$ (**1**) was prepared from **bis(*n*-octadecylcarboxy)ethylamine (2).** Di-*n*-octadecylamine (Fluka) (5.2 g, 10 mmol) and 2.1 mL (15 mmol) of triethylamine were dissolved in 50 mL of ethyl ether and 20 mL of methylene chloride; to this stirred solution, cooled in a water bath, 1.3 g (12 mmol) of ethyl chloroformate was slowly added (ca. 15 min.). The resulting suspension was further stirred for 30 min at room temperature and then washed with 0.1 N HCl, 0.1 N NaOH, and water. The solvent was dried and removed under vacuum. The remaining oil was crystallized from acetone in a refrigerator and gave 4.8 g (yield 81%) of **2**: mp 42 °C; ^{1}H NMR ($CDCl_3$) δ 4.00 (q, 2 H), 3.15 (br t, 4 H), 1.0-1.6 (br s, 64 H), 0.90 (t, 6 H).

Di-*n*-octadecylmethylamine (3). **2** (4.0 g, 6.7 mmol) dissolved in 20 mL of anhydrous ethyl ether was added at room temperature to a stirred suspension of 1.0 g (26 mmol) of $LiAlH_4$ in 30 mL of ethyl ether. The resulting mixture was refluxed for 24 h. The excess of $LiAlH_4$ was destroyed with 15% NaOH and the resulting inorganic hydroxide filtered. The added solvent was removed under vacuum and **3** crystallized from acetonitrile: 3.28 g (yield = 91%); mp 35 °C; ^{1}H NMR ($CDCl_3$) δ 2.05-2.50 (br t + s, 7 H), 1.0-1.6 (br s, 64 H), 0.90 (t, 6 H).

4-Chloromethylstyrene (4) was prepared according to the literature:[25] bp 93 °C; ^{1}H NMR CCl_4) δ 7.20 (br s, 4 H, aromatic), 4.9-6.9 (m, 3 H, vinyl), 4.40 (s, 2 H).

Bis(*n*-octadecylmethyl)(*p*-vinylbenzyl)ammonium Chloride 1. **3** (1.4 g, 2.6 mmol) 0.4 g (2.6 mmol) of **4**, and 0.05 g of *tert*-butylcatechol were heated for 48 h at 70 °C in the absence of solvent. The reaction mixture was treated in methylene chloride with aqueous 0.1 N NaOH; drying and removal of the solvent and then addition of pentane gave **1**, 0.7 g (yield = 40%). **1** was recrystallized from ethyl acetate: mp 118-135 °C; ^{1}H NMR ($CDCl_3$) δ 7.50 (d d, 4 H), aromatic), 5.1-6.9 (m, 3 H, vinyl), 5.05 (br s, 2 H), 3.1-3.6 (br m + br s, 7 H), 1.0-1.9 (br s, 64 H), 0.9 (t, 6 H).

Trisodium 8-hydroxy-1,3,6-pyrenetrisulfonate, POH (Eastman), was recrystallized three times from aqueous acetone (5:95, v/v) using charcoal. Thin-layer chromatography on Merck G-F 254 plates showed only one spot (*n*-C_4H_9OH:H_2O = 6:1, v/v, as eluent). 2-Aminopyridine (Aldrich) was recrystallized from pentane. HCl and NaOH were used to adjust the pH to the required value. Dimethyldioctadecylammonium bromide (Eastman) was recrystallized from acetone. The recrystallized sample was passed through an anion exchange column (chloride form, BioRad Lab, AG2-X, 20-50 mesh) using MeOH-$CHCl_3$ (70:30 v/v) as eluent. The solution was evaporated to dryness and passed once again through a fresh anion exchange column. The solid, resulting from evaporation to dryness, was recrystallized three times from ethylacetate. The product, dimethyldioctadecylammonium chloride (DODAC), was found to be free of amine hdyrochloride by IR and NMR spectroscopy. No bromide ion was detected in DODAC by magenta test. Sephadex G-50 (Sigma) was used as received.

Deionized water was doubly distilled in an all-glass apparatus. The final stage of distillation included a superheated oxygenated quartz column. Additionally, double-distilled water was filtered through a 0.2-μm Millistak filter system (Millipore Corp.). Usually, it gave a pH of 5.5 **1** (10 mg) was dissolved in 0.2 mL of MeOH to which 20 mL of dustless water was added. The sample was then sonicated at 75 °C by using the medium tip of the Braunsonic 1510 sonicator set at 70 W for different times. Vesicles used for polymerization and for detailed studies have been sonicated for 60 min and filtered through a 0.2-μm Nucleopore filter. These vesicle solutions were completely transparent and had hydrodynamic radii of 425 ± 25 Å. DODAC vesicles were prepared in a similar manner. A Radiometer pHM26 meter was used, in conjunction with a combination microelectrode for pH determinations.

Absorption spectrophotometry were carried out either on a Cary 118C and/or on a Hewlett Packard 8450 A Diode Array spectrophotometer. Fluorescence spectra and polarization were recorded on a Spex Fluorolog spectrofluorometer.

Fluorescence lifetimes and time-resolved fluorescence anisotropies were determined on a single photon counting system using tunable laser pulses as the excitation source. A Spectra-Physics cavity dumped rhodamine 6G dye laser syncronously pumped by a mode locked argon ion laser (No. 171) was used to provide tunable 15-ps pulses at 0.8 MHz. The second harmonic (296 nm, vertically polarized) was generated by means of a temperature-tuned ADA crystal. The residual 592-nm radiation was removed by a 7-54 Corning glass cutoff filter. The ORTEC 457 TAC was used in the normal mode. The "start" signal was obtained from a portion of the 592-nm pulses via a Texas Instrument TIED 56 photodiode and an ORTEC 436 discriminator. The emission signal, viewed at 90° and passed through an ultraviolet Polacoat polarizer (OM type 105, uv VRMR) set at 54.7° for lifetime and 0° ($I_\parallel(t)$) or 90° ($I_\perp(t)$) for anisotropy determinations, was used to stop the TAC. Photon counting and data treatment by the Marquardt algorithm have been previously described. Precision of the fit was estimated by the χ^2 parameter and by inspecting the residuals and matrix covariances.

Flash photolysis measurements were carried out by using the third (353 nm) and fourth harmonics (266 nm) of a Nd:YAG laser (Quanta Ray DCR-1A) for excitation and a xenon lamp (150 W Oriel) for the analyzing light. A manual trigger provided the start signal for opening a fast shutter between the xenon lamp and the sample cell, triggering the fast digitizer (Tektronix RF912), and dropping the electrooptical Q switch in the laser cavity to zero potential, thus firing the laser. An adjustable delay box allowed the time between digitizer triggering and laser firing to be selected so that the prelaser-pulse light level transmitted through the sample appeared on the waveform as well as the suceeding laser-induced events. The pulse of 15 ns fwhm was used at an energy level of approximately 10 mJ/pulse as measured by a Scientech disk power meter (36-2002) operating as a surface absorber, rather than as a volume absorber. An optical train of ultraviolet transmitting lenses focused the collimated xenon lamp light into the sample cell and refocused the transmitted light onto the entrance slit of a Jarrell-Ash 25-cm monochromator equipped with low blaze for ultraviolet measurements.

(5) Fendler, J. H. *Science* **1984**, *223*, 888-894.
(6) Gros, L.; Ringsdorf, H.; Schupp, H. *Angew. Chem., Int. Ed. Engl.* **1981**, *20*, 305-325.
(7) Fendler, J. H. In "Surfactants in Solution"; Mittal, K. L., Lindman, B., Eds.; Plenum Press: New York, 1984, 1947-1989.
(8) Fendler, J. H.; Tundo, P. *Acc. Chem. Res.* **1984**, *17*, 3-7.
(9) Fuhrhop, J. H.; Mathieu, J. *Angew. Chem., Int. Ed. Engl.* **1984**, *23*, 100-113.
(10) Regen, S. L.; Czech, B.; Singh, A. *J. Am. Chem. Soc.* **1980**, *102*, 6638-6940.
(11) Barraud, A.; Rosillo, C.; Ruadei-Teixier, A. *J. Colloid Interface Sci.* **1977**, *62*, 509-563.
(12) Johnson, D. J.; Snaghera, J.; Pons, M.; Chapman, D. *Biochem. Biophys. Acta* **1980**, *602*, 57-69.
(13) Paleous, C. M.; Christias, C.; Evangelatos, G. P.; Dais, P. *J. polym. Sci. Polym. Chem. Ed.* **1982**, *20*, 2565-2573.
(14) Dorm, K.; Klingbiel, K. T.; Specks, D. P.; Tyminski, P. N.; Ringsdorf, H.; O'Brien, D. F. *J. Am. Chem. Soc.* **1984**, *106*, 1627-1633.
(15) Ishiwatari, T.; Fendler, J. H. *J. Am. Chem. Soc.* **1984**, *106*, 1908-1912.
(16) Reed, W.; Guterman, L.; Tundo,, P.; Fendler, J. H. *J. Am. Chem. Soc.* **1984**, *106*, 1897-1907.
(17) Roks, F. M. M.; Visser, H. G. S.; Zwikker, J. W.; Verkley, A. J.; Nolte, R. J. M. *J. Am. Chem. Soc.* **1983**, *105*, 4507-4514.
(18) Reed, W.; Hauser, H.; Fendler, J. H. *J. Am. Chem. Soc.*, in press.
(19) Kano, K.; Fendler, J. H. *Biochim. Biophys. Acta* **1978**, *504*, 289-299.
(20) Huppert, D.; Gutman, M.; Kaufmann, K. J. *Adv. Chem. Phys.* **1981**, *47*, 643-679.
(21) Pines, E.; Huppert, D. *J. Phys. Chem.* **1983**, *87*, 4471-4478.
(22) Forster, Th.; Volker, S. *Chem. Phys. Lett* **1975**, *34*, 1-6.
(23) Escabi-Perez, J. R.; Fendler, J. H. *J. Am. Chem. Soc.* **1978**, *100*, 2234-2236.
(24) Politi, M.; Fendler, J. H. *J. Am. Chem. Soc.* **1984**, *106*, 265-273.

Table I. Hydrodynamic Radii of Vesicles and Polymerized Vesicles Prepared from 7.2×10^{-4} M **1** Under Different Conditions

	θ, deg	R_H, Å	Q value
sonicated			
2 min	90	>2000	0.85
15 min	90	1680	0.53
30 min	90	931	0.35
45 min	90	550	0.19
60 min	90	425	0.15
75 min	90	425	0.15
60 min	60	510	0.14
60 min	75	479	0.16
60 min	105	428	0.13
sonicated for 60 min after 1 day of incubation	90	425	0.15
sonicated for 60 min after 1 week of incubation	90	429	0.13
sonicated for 60 min and polymerized	90	432	0.16
	60	506	0.13
	75	480	0.17
	105	420	0.14
sonicated for 60 min, polymerized and incubated for days	90		

A Hammamatsu R928 phototube was used for measuring the light level transmitted through the sample cell. The phototube divider network used a short five-dynode plan for fast response and artifact-free operations. The tektronix digitizer was interfaced to a DEC PDP11/34A minicomputer. The minicomputer controlled the digitizer. Software has been developed for signal averaging, final data reduction, analysis, and graphics.[26]

The 266-nm laser pulses were also utilized for affecting vesicle photopolymerization.[16] The loss of styrene absorbance was monitored as a function of the absorbed laser energy.

Static and dynamic light scattering were determined on a Brookhaven Instrument (goniometer, digital correlator, microcomputer), using a Spectra Physics 171 Argon ion laser as the excitation source.[16,27]

Results

Characterization of Vesicles Prepared From 1. Ultrasonic dispersal of **1** above its phase transition temperature resulted in aggregate formation. Increasing the time of sonication led to progressively smaller and more monodisperse vesicles (Table I). Sonicated **1** vesicles could not be passed through Diaflow YM 30 filters (cutoff 30 000); no monomeric surfactant **1** could be detected in the filtrate. Formation of aggregates was substantiated by gel filtration on Sephadex G-50. The aggregates, monitored absorption photometrically at 254 nm, appeared in the void volume of the column. It should be pointed out, however, that substantial amounts of **1** were adsorbed on the column.

The presence of closed vesicles was demonstrated by entrapping 2-aminopyridinium chloride, 2AP, at pH 3.0. 2AP was entrapped by cosonication with **1** to give a stoichiometric solution of [**1**] = 7.2×10^{-4} M and [2AP] = 1.0×10^{-2} M. Electrostatic repulsions between the positively charged head groups of **1** vesicles and 2AP ensured the entrapment of this probe well within the water pools of the vesicles. Unentrapped 2AP was removed by exhaustive dialysis (using diaflow YM 30 filters) until no 2AP could be detected in the filtrate (by fluorescence spectroscopy λ_{ex} = 290 nm, λ_{em} = 395 nm). 2AP was detected, however, in **1** vesicles subsequent to exhaustive dialysis. Injecting 0.10 mL of 0.10 M NaOH to 3.0-mL solutions of **1** vesicle entrapped 2AP resulted in the immediate (30 s, the time needed for making the measurements) loss of fluorescence, indicating the prompt permeability of hydroxide ions across the vesicle bilayers. Addition of 0.10 mL of 0.10 M HCl restored the initial fluorescence showing the equally facile proton permeability.

As seen in Table I, under the present experimental conditions, 60 min of sonication led to optimal sized vesicles and monodispersities. The sizes of these 60 min sonicated vesicles remained unaltered for weeks.

(25) Arshady, R.; Ledwith, A. *Makromol. Chem.* **1978**, *179*, 819–822.
(26) Reed, W. Ph. D. Dissertation, Clarkson University, 1984.
(27) Chu, B. "Laser Light Scattering", Academic Press: New York, 1974.

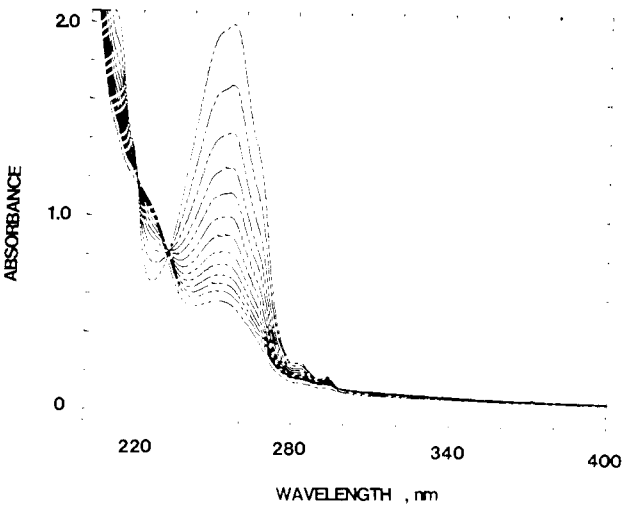

Figure 1. Absorption spectra of 425 ± 20 Å radius vesicles prepared from **1**. Each succeeding lower curve was taken after an additional 100 1-mJ laser pulses at 266 nm. Increasing irradiation results in decreased absorbances at 250 nm.

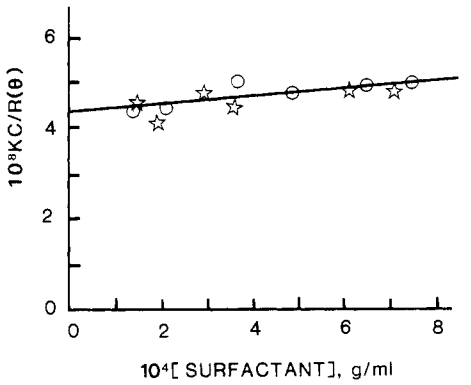

Figure 2. Plots of static light scattering data at 90° for nonpolymerized 425 ± 20 Å (circles) and polymerized (stars) vesicles prepared from **1**, according to eq 1.

Vesicle Photopolymerization. Absorption spectra of **1** vesicles (425 ± 25 Å radii) prior and subsequent to exposure to increasing amounts of laser energy are shown in Figure 1. Photoexcitation is seen to lead to an exponential decrease of the styrene absorbance indicating the photopolymerization of **1** vesicles.[16]

Molecular Weights of Vesicles and Polymerized Vesicles. Weight averaged molecular weights, $\bar{M}_w$, of vesicles and polymerized vesicles were determined by static light scattering with use of eq 1

$$\frac{Kc}{R_\theta} = \frac{1}{\bar{M}_w} + 2Bc \tag{1}$$

where c is the concentration of **1** in g/mL, B is the second virial coefficient, and K and the Rayleigh ratio, R_θ, are given by

$$K = \frac{2\pi^2 n^2 (dn/dc)^2}{N_A \lambda^4} \tag{2}$$

$$R_\theta = \frac{i_s r^2}{I_0(1 + \cos^2\theta)} \tag{3}$$

where n is the refractive index of the solvent (taken to be that of water, 1.33), dn/dc is the refractive index increment (0.108), N_A is Avogardro's number, λ is the wavelength of laser excitation (514 nm), i_s is the intensity of the light scattered per unit volume, I_0 is the intensity of the incident light, θ is the angle of observation (90°), and r is the distance from the scatter cell to the analyzer. When static light scattering was used, the vesicle solution gave only a weak angular dependence for the scattered light, as expected

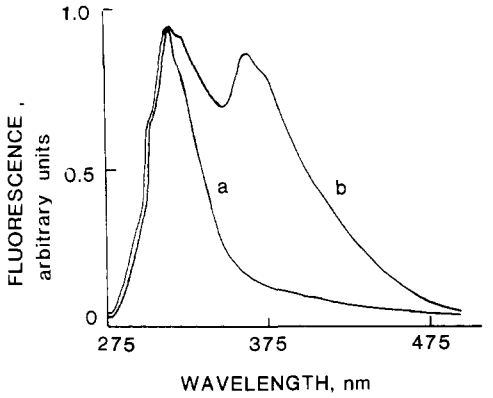

Figure 3. Emission spectra of nonpolymerized (a) and polymerized (b) 425 ± 25 Å vesicles prepared from **1**. λ_{ex} = 275 nm.

Table II. Fluorescence Decay Times (τ_1 and τ_2) and Anisotropies (τ_R) of Vesicles and Polymerized Vesicles Prepared from **1**[a]

	observation wavelength, nm	τ_1, ns	τ_2, ns	τ_R,[b] ns
nonpolymerized **1**	315	0.52	1.71	1.29 (0.045)
polymerized **1**	315	0.70	3.83	3.02 (0.27)
	440	1.06	3.18	4.17 (0.25)

[a] R_H = 425 ± 25 Å for nonpolymerized and polymerized vesicles. Error in lifetimes ±10%, error in τ_R ±30%, λ_{ex} = 295 nm. [b] Values in parentheses are residual polarizations.

since the diameter of the particle (ca. 80 nm) is only about 15% of the wavelength of the incident light (514 nm) so that the vesicles act like Rayleigh scatterers to a reasonable approximation. Data were, therefore, only taken at 90°. Figure 2 shows plots of data according to eq 1 for 425 ± 25 Å radii nonpolymerized and photopolymerized vesicles prepared from **1**. Substituting appropriate constants led to $2.33 \times 10^7 \pm 4\%$ and $2.32 \times 10^7 \pm 4\%$ for $\bar{M}_w$ with a second virial coefficient of $8.7 \times 10^{-6} \pm 43\%$ of nonpolymerized and polymerized **1** vesicles. Combining these values with the molecular weight of monomeric **1** (687.5) indicated that each vesicle contains 34 000 surfactant molecules. Substitution into

$$S_A = \frac{4\pi R_{H,0}^2 + 4\pi R_{H,i}^2}{34\,000} \qquad (4)$$

where $R_{H,0}$ and $R_{H,i}$ are the hydrodynamic radii of the vesicles (425 Å) and of vesicle entrapped water pools (375 Å), led to 118 Å^2 for the surface area per monomer (S_A) in the vesicles. This value should be compared with those previously determined for vesicles prepared from a similar surfactant, $[n\text{-}C_{15}H_{31}CO_2\text{-}(CH_2)_2]_2N^+(CH_3)CH_2C_6H_4CH{=}CH_2, Cl^-$ (94 Å^2)[16] and for phospholipid liposomes (74 Å^2).[28] It is important to emphasize that neither the hydrodynamic radii nor the weight averaged molecular weights of vesicles, prepared from **1**, changed upon polymerization. Addition of POH to nonpolymerized vesicles did not appreciably change the hydrodynamic radii or the diffusion coefficients of the vesicles.

Steady-State and Subnanosecond Time-Resolved Fluorescence and Fluorescence Polarization of Vesicles and Polymerized Vesicles. Excitation of surfactant vesicles prepared from **1** at 275 nm resulted in fluorescence with an emission maximum at 310 nm (Figure 3). Identical fluorescence spectra were observed in a 1.0×10^{-5} M ethanolic solution of **1**. The fluorescence originates, of course, in the styrene moiety. Upon polymerization the fluorescence spectrum of **1** vesicles changed. A new emission maximum appeared at 370 nm, due to excimer formation. Concomitantly, emission intensity of the 310-nm band decreased (Figure 3).

Table II collects fluorescence lifetimes and time-dependent fluorescence anisotropies for the styrene moiety of nonpolymerized and polymerized **1** vesicles. Upon polymerization both of these lifetimes were found to increase. Importantly, within the time scale of observation rotational reorientations were incomplete. For nonpolymerized vesicles there were residual anisotropies of about 0.045, whereas for polymerized **1** vesicles the majority of the anisotropy signal was a residual of about 0.25–0.27.

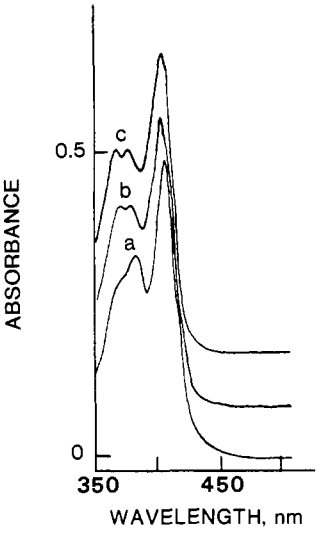

Figure 4. Absorption spectra of 2.2×10^{-5} M POH in nonpolymerized vesicles (a), in water (b), and in polymerized vesicle (c); all at pH 4.78.

Interaction of POH with Vesicles and Polymerized Vesicles. These experiments were carried out by injecting appropriate concentrations of POH solutions to already formed or to already polymerized **1** vesicles. Absorption spectra of POH in nonpolymerized and polymerized **1** vesicles show the characteristic maxima due to the protonated and ionized forms of POH (eq 5):[23,24]

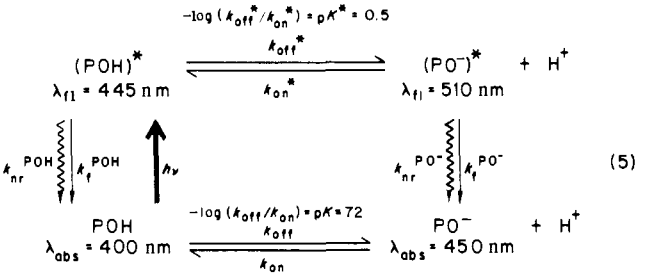

Absorption maxima of the protonated form of POH in water, in nonpolymerized and polymerized **1** vesicles are shown in Figure 4. The absorption maxima of POH shifted to 408 nm in the vesicles. Bands in the 360–390 region are sensitive to the environment and show similarities between water (Figure 4b) and polymerized (Figure 4c) vesicles, while those in nonpolymerized vesicles (Figure 4a) are similar to those in methanol and CTAB micelles.[28]

Excitation of POH, following immediately its addition to nonpolymerized vesicles ([**1**] = 7.2×10^{-4} M, [POH] = 1.0×10^{-5} M; stoichiometric concentrations) at 408 nm resulted in fluorescence emission with maxima at 440 and 520 nm (Figure 5). Fluorescence intensities of POH in nonpolymerized and polymerized **1** vesicles were, however, some 14- and 15-fold lower than that in water under identical conditions. (A similar 5-fold decrease in fluorescence intensity was observed in comparing fluorescence intensity of POH in DODAC vesicles with that in water.) Incremental addition of POH to nonpolymerized **1** vesicles did not result in an increase of fluorescence intensity until the stoichiometric POH concentration reached 2.0×10^{-4} M. This corresponded to the complete coverage of the outer surface of **1** vesicles ([**1**] = 7.2×10^{-4} M). Further POH addition caused an exponential increase of POH fluorescence intensity to a level

(28) Huang, C.; Mason, J. T. *Proc. Natl. Acad. Sci. U.S.A.* **1978**, *75*, 308–310.

Table III. Fluorescence Decay Times (τ_{off}, τ_1, τ') and Anisotropies (τ_R) of POH in Nonpolymerized and Polymerized 1 Vesicles at Different Incubation Times[a]

	observation wavelength, λ_{nm}	f	τ_{off}, ns	τ, ns	τ', ns	τ_R,[b] ns	$10^9 k_{off}$*, s^{-1}	$10^9 k_{on}'$*, s^{-1}
nonpolymerized 1								
30 minutes after injection	445	0.95	0.42	1.55			4.3	0.087
	510			1.42[c]	3.90	≥50 (0.12)		
1 day after injection	445			1.38	4.02[c]	≥50 (0.14)		
	510			1.38[c]	3.80			
polymerized 1								
30 min after injection	445	0.92	0.68	3.60			6.3	0.096
	510			2.98[c]	6.40	4.54 (0.023)		
1 day after injection	445	0.91	0.74	3.50			6.4	0.096
	510			2.83[c]	6.57	3.45 (0.321)		

[a] R_H = 420 ± 25 Å for both polymerized and nonpolymerized vesicles. 1.0×10^{-5} M POH added to nonpolymerized and polymerized 1 vesicles, prepared from 7.2×10^{-4} M surfactant by sonication. Error in lifetimes ±10% and in anisotropies ±30%. [b] Values in parentheses are residual polarizations. [c] Incomplete spectral resolution of (POH)* and (PO^-)* fluorescences.

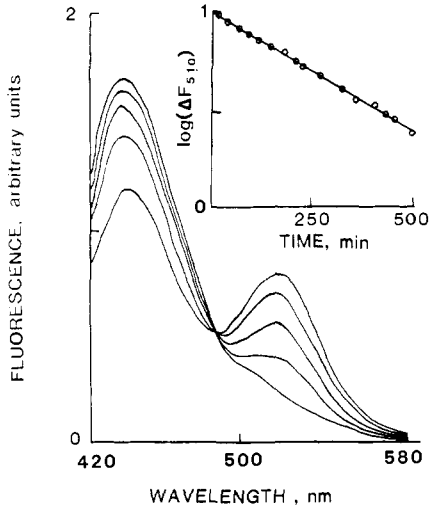

Figure 5. Fluorescence spectra of POH at different times to its addition to nonpolymerized vesicles prepared from 1. Spectra at times 0, 90 min, 240 min, 480 min, and 24 h illustrate the increasing fluorescence at 440 nm and the concomitant decrease of the 250-nm band. Time dependence of this process is shown in the insert.

observed in water. These results imply the appreciable association of POH with vesicles and that this association is somewhat stronger in nonpolymerized than in polymerized 1 vesicles.

As seen in Figure 5, incubation of POH in 1 vesicles led to time-dependent changes of the fluorescence spectra. Increasing incubation time resulted in the gradual disappearance of the emission band at 520 nm and in the concomitant increase of the emission band at 440 nm. The time-dependent disappearance of the 520-nm POH fluorescence band is plotted in the insert in Figure 5. The $1/e$ time of this process was calculated to be ca. 440 min.

Conversely to nonpolymerized 1 vesicles, fluorescence spectra of POH did not show any time-dependent changes following its addition to polymerized 1 vesicles (Figure 6).

Excited-State Protonation Equilibria of POH in Vesicles and Polymerized Vesicles. Differences between nonpolymerized and polymerized 1 vesicles are also manifested in the time-dependent excited-state protonation equilibria of POH (eq 5 in them). Fluorescence lifetimes of (POH)* and (PO^-)* are given by

$$-\frac{d[(POH)^*]}{dt} = (k_{off}^* + k_f^{POH} + k_{nr}^{POH})[(POH)^*] - k_{on}^*[(PO^-)^*][H^+] \quad (6)$$

$$-\frac{d[(PO^-)^*]}{dt} = (k_f^{PO^-} + k_{nr}^{PO^-})[(PO^-)^*] + k_{on}^*[(PO^-)^*][H^+] - k_{off}^*[(POH)^*] \quad (7)$$

With the adjustment of the pH such that all ground-state population is protonated (say pH 5), integration of eq 6 and 7 leads to

$$[(POH)^*] = [(POH)^*]_0 e^{-t/\tau} \quad (8)$$

$$[(PO^-)^*] = \frac{k_{off}^*[(POH)^*]_0(e^{-t/\tau'} - e^{-t/\tau})}{k_{off}^* - k_{on}^*[H^+] + k_f^{POH} - k_f^{PO^-} + k_{nr}^{POH} - k_{nr}^{PO^-}} \quad (9)$$

where τ and τ' are the lifetimes of (POH)* and (PO^-)* at $pK_a^* < pH < pK_a$, and

$$\tau = \frac{1}{k_{off}^* + k_f^{POH} + k_{nr}^{POH}} \quad (10)$$

$$\tau' = \frac{1}{k_f^{PO^-} + k_{nr}^{PO^-}} \quad (11)$$

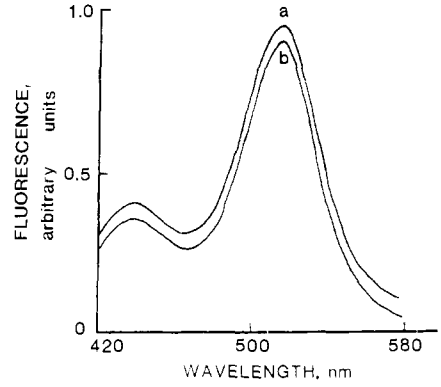

Figure 6. Fluorescence spectra of POH 10 min (a) and 1 day (b) subsequent to its addition to polymerized vesicles prepared from 1.

Figure 7 shows fluorescence lifetimes, monitored at 445 and 510 nm, in nonpolymerized and polymerized vesicles within 30 min of the addition of POH and 1 day subsequent to it. Lifetimes observed at 445 nm were resolved into faster, τ_{off} (0.4–0.7 ns), and slower, τ (1.4–3.0 ns), components (Table III). Lifetimes of the slower components, attributable to (POH)* fluorescence, are markedly shorter than those found in water (5.2 ns), and aqueous (3.0 ns) and reversed (3.7 ns) micelles.

Fluorescence lifetimes measured at 445 nm allow the calculation of k_{off}^* and k_{on}^* ($k_{on}^* = k_{on}^*[H^+]$) from[29]

$$k_{off}^* = f\frac{1}{\tau_{off}} + (1-f)\frac{1}{\tau} - (k_f + k_{nr}) \quad (12)$$

$$k_{on}'^* = (1-f)\left(\frac{1}{\tau_{off}} - \frac{1}{\tau}\right) \quad (13)$$

where f is the fraction of the fast-decaying component of the total

(29) Politi, M.; Brandt, O.; Fendler, J. H. J. Am. Chem. Soc., in press.

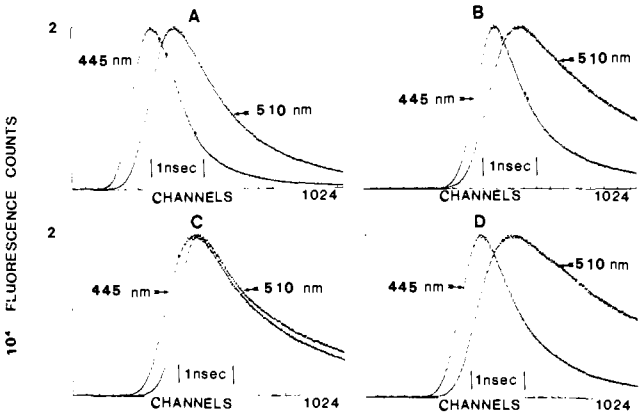

Figure 7. Fluorescence buildup and decay plots of 1.0×10^{-5} M POH in vesicles prepared from 70×10^{-4} M **1** at pH 4.78 and ambient temperature. Plotted are the fluorescence intensities in terms of counts of the multichannel analyzer vs. channel number (0.005 ns (channel)). Upper and lower represent nonpolymerized and polymerized vesicles, respectively, immediately after the addition of POH; C and D were taken for nonpolymerized and polymerized vesicles 24 h subsequent to the addition of POH.

concentration of (POH)*. Table III contains the calculated values.

Alternatively, k_{off}* can also be derived from[30]

$$\Delta t = \frac{\ln (k_{off}^{*}\tau)}{k_{off}^{*} - \tau^{-1}} \qquad (14)$$

where Δt is the time lag between the peaks of (POH)* and (PO^-)* emission decays. Figure 7 indicates the time lags for maximal count (normalized to 20 000) between direct fluorescence, $PO^- + h\nu \rightleftharpoons (PO^-)^*$, and that via proton ejection, $(POH)^* \rightarrow (PO^-)^* + H^+$. Substituting these values into eq 14 gave k_{off}* values of 4.3×10^9 and 6.1×10^9 s^{-1} for (POH)* deprotonation in nonpolymerized and polymerized **1** vesicles *immediately after the injection of POH* to the vesicles. These values of k_{off}* agree well with those calculated from eq 12 (Table III) and hence concur with those derived by Gutman and co-workers.[20,29] k_{off}* values in nonpolymerized and polymerized vesicles are, however, somewhat closer to that determined in water (8.9×10^9 s^{-1}) than that obtained in aqueous micelles (4.8×10^8 s^{-1}).[24] Incubation for a day did not influence the rate of excited-state proton ejection from (POH)* in polymerized **1** vesicles (see Table III and compare Δt values in Figure 7 for polymerized **1** vesicles at different times). Conversely in nonpolymerized **1** vesicles, following a day of POH incubation excited-state proton ejection could not be observed (compare Δt values in Figure 6 at different times and note the absence of τ_{off} value in nonpolymerized vesicles a day after POH injection).

Fluorescence lifetimes observed at 510 nm were also resolved into two components. The longer lived major component (3.9 ns in nonpolymerized and 6.4–6.6 ns in polymerized **1** vesicles) is due to (PO^-)* decay. The shorter lived minor components are similar to those observed at 445 nm and are the consequence of incomplete spectral resolution of (POH)* and (PO^-)* fluorescences.

Steady-State and Time-Resolved Fluorescence Polarization of (POH)* in Vesicles and Polymerized Vesicles. Steady-state fluorescence polarizations of (POH)* subsequent to its addition to nonpolymerized and polymerized **1** vesicles as functions of incubation time are collected in Table IV. Environments of the probe are seen to be appreciably less hindered in polymerized than in nonpolymerized vesicles. Importantly, polarizations in polymerized vesicles do not change with incubation time, whereas the POH reports progressively more hydrophobic environments.

Time-resolved fluorescence anisotropies of (POH)* are also given in Table III. The (POH)* is immobilized in the unpolymerized vesicles with a τ_R greater than 50 ns; i.e., τ_R is far too long to be accessible to this anisotropy technique, and may well be on the order to the entire vesicle rotational reorientation lifetime. The residuals (in parentheses) of the (POH)* anisotropy are high, agree well with the steady-state values in Table IV, and indicate that the (POH)* is fairly well immobilized in the unpolymerized vesicles. In polymerized vesicles, on the other hand, Table III indicates a measurable τ_R of roughly 4.0 ns and negligible residuals for (POH)*. Steady-state values in Table IV confirm this. (POH)* is thus free to reorient fairly rapidly in polymerized vesicles.

Table IV. Steady-State Polarizations of (POH) in Nonpolymerized and Polymerized **1** Vesicles at Different Incubation Times[a]

	polarization in **1** vesicles[b]	
incubation time	nonpolymerized	polymerized
2 min	0.12	0.078
1 h	0.12	
3 h	0.15	
5 h	0.17	
30 h	0.19	0.074
50 h	0.19	0.080

[a] $R_H = 425 \pm 20$ Å for both nonpolymerized and polymerized vesicles. 1.0×10^{-5} M POH added to nonpolymerized and polymerized vesicles prepared from 7.2×10^{-4} M surfactants by sonication. [b] POH polarization in 0.25 M CTAB at pH 9.8 is 0.19 and at pH 2.09 it is 0.14.[19] POH polarization in water is 0.016.[19]

Ground-State PO^- Reprotonations in Vesicles and Polymerized Vesicles. Excitation of $(2–6) \times 10^{-5}$ M POH in **1** vesicles by a 2–5-mJ 353-nm laser pulse resulted in the transient formation of PO^- and H^+. This could be seen in the prompt (unmeasurably fast under our experimental conditions) bleaching of the ground-state POH absorbance at 400 nm and the parallel development of the PO^- absorbance at 450 nm. Subsequent decay of the PO^- absorbance, monitored at 450 nm, or the recovery of the POH absorbance, monitored at 400 nm, occurred on the microsecond time scale. This process, corresponding to the ground-state reprotonation of PO^- (see k_{on} in eq 5), is expressed by

$$-\frac{d[PO^-]}{dt} = \frac{d[POH]}{dt} = k_{on}[PO^-][H^+]_t \qquad (15)$$

where $[H^+]_t$, the total hydrogen ion concentration, is the sum of bulk and ejected hydrogen ion concentrations

$$[H^+]_t = [H^+]_{bulk} + [H^+]_{ejected} \qquad (16)$$

and, if initially there was only POH (pH < pK − 1), then

$$[H^+]_{ejected} = [PO^-]_t \qquad (17)$$

and eq 13 becomes

$$-\frac{d[PO^-]}{dt} = k_{on}[PO^-]([PO^-] + [H^+]_{bulk}) \qquad (18)$$

which upon integration and rearrangements leads

$$\frac{1}{[H^+]_{bulk}} \ln\left(\frac{[H^+]_{bulk}}{[PO^-]} + 1\right) + C = k_{on}t \qquad (19)$$

Figure 9 shows a typical digitized trace for the laser pulse initiated PO^- reprotonation and plots of the data according to eq 19. Typically, 15–20 individual shots were averaged for each final data trace. Computer program KINF was used for calculating k_{on} values.[26,29] The effect of laser pulses on pyrene degradation was assayed by continuously monitoring the absorption spectra of the samples. Values of k_{on} are collected in Table V. It should be noted that bulk proton concentrations were used as determined by a pH meter. Reprotonation rates represent, therefore, apparent values. The significant point to note is, however, that while proton

(30) Tsujii, K.; Sunamoto, J.; Nome, F.; Fendler, J. H. *J. Phys. Chem.* **1978**, *82*, 423–429.

Table V. Rate Constants for Laser pH-Jump Initiated PO^- Reprotonations in Nonpolymerized and Polymerized **1** Vesicles at Different Incubation Times

	pH	$10^{-8}k_{on}$,[a] M^{-1} s^{-1}
Nonpolymerized **1**		
30 min after injection	4.15	4.4
	4.15	3.7
	4.42	4.2
1 day after injection	4.15	not measurable
	4.42	not measurable
Polymerized **1**		
30 min after injection	3.90	8.3
	4.40	6.0
	4.86	7.9
1 day after injection	4.20	8.7
	4.15	7.1

[a] k_0n in H_2O at $\mu_0 = 1.26 \times 10^{11}$ M^{-1} s^{-1}. k_{on} in CTAB = 4×10^9 M^{-1} s^{-1}.[24]

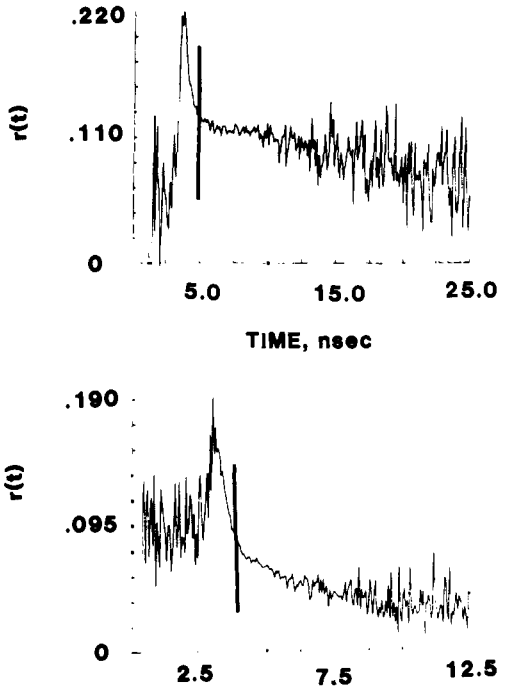

Figure 8. (A, top) Time-resolved anisotropy $r(t)$ of POH in unpolymerized vesicle, about $^1/_2$ h after injection; (B, bottom) $r(t)$ for POH in polymerized vesicle, 1 day after injection. Initial peak in both curves is artefactual and is due to the instrument response pulse. Analysis starts at the vertical bar drawn on the graphs.

ejection could be affected in freshly prepared and incubated polymerized **1** vesicles, in nonpolymerized vesicles they could only be observed within a short time after the POH injection. No PO^- reprotonation could be measured in incubated nonpolymerized **1** vesicles.

Discussion

Significant morphological changes have been observed upon the surface photopolymerization of vesicles prepared from surfactants which contain styrene in their head groups. Thus, while the permeability of pyranine in nonpolymerized vesicles is relatively unhindered, it is apparently alleviated upon polymerization. Negatively charged POH, subsequent to its injection, is likely to bind to the positively charged head groups of nonpolymerized vesicles. This may lead to some increased self absorbance which was manifested in decreased fluorescence intensity. Since the head-group region of the vesicle is extensively hydrated, POH retains its proton ejection properties. In time, the hydrophobic forces overcome the electrostatic attractions and POH begins to work its way into the vesicle bilayer. Not unexpectedly, this

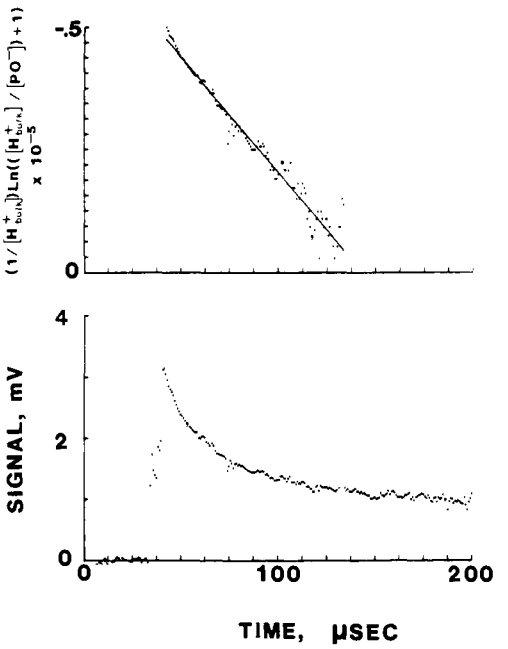

Figure 9. Digitized plot of the absorbance changes at 450 nm following PO^- reprotonation ([POH] = 1.0×10^{-5}) in vesicles prepared from 7.0×10^{-4} M **1** at pH 4.15; excitation by 8-mJ 353-nm pulses (bottom); treatment of the data according to eq 17 (top).

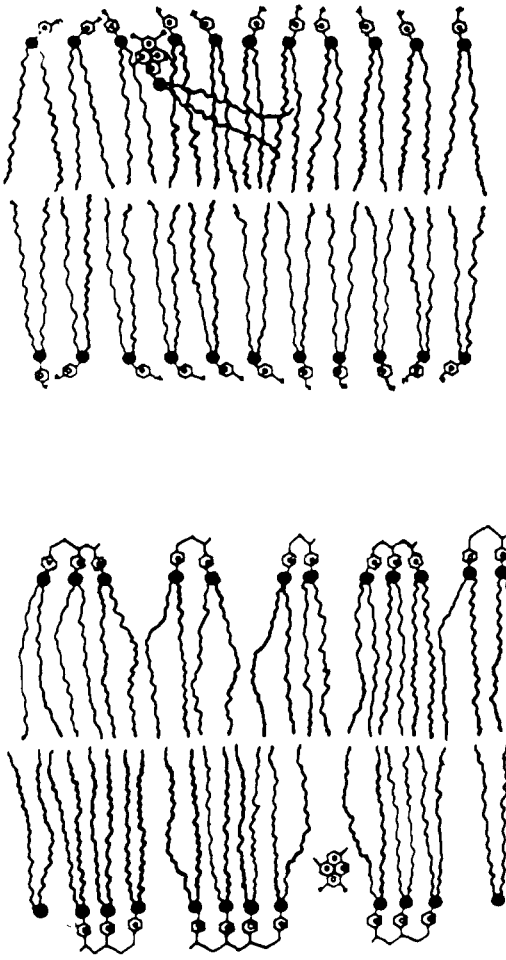

Figure 10. Artist's conception of interaction between POH and nonpolymerized (top) and polymerized (bottom) vesicles prepared from **1**.

process is rather slow. Ultimately, POH is completely engulfed in the vesicle bilayer to such an extent that it can no longer ionize in the excited state. Similar behavior of POH has been observed

in apolar solvents and in reversed micelles which contained no free water molecules.[20,29]

The behavior of pyranine in polymerized vesicles is entirely consistent with the proposed cleft formation which results from the pulling together of the head groups upon surface polymerization. The clefts are conceived of as water-filled pockets of exposed hydrocarbon chains on the vesicle surface. Electrostatic and hydrophobic interactions are responsible for pulling POH into and subsequently retaining it in the clefts of polymerized **1** vesicles. Polymerization prevents the deeper penetration of POH into the vesicle bilayer. Indeed, the whole nature of the bilayer has been altered by the photopolymerization induced surface inhomogeneity. POH can remain solubilized indefinetely in the clefts and maintain its stable, noncovalent association with the vesicles. An artists's conception of POH interaction with nonpolymerized and polymerized vesicles prepared from **1** is shown in Figure 10.

Results of anisotropy measurements also support the proposed morphological changes upon vesicle photopolymerization. Rotation of POH is more hindered and less complete in unpolymerized than in polymerized vesicles (Table III). The residual polarization of POH in nonpolymerized vesicles (ca. 0.1) indicates that POH is only able to reorient about a certain axis rather than tumble freely. In contrast, in the polymerized vesicles the POH is able to reorient almost entirely, which is consistent with the idea that the POH is water solubilized in a relatively large surface cleft on the vesicle. The fact that τ_R (ca. 4 ns) is much larger than in pure water (<100 ps, and unresolvable by our experiment) indicate that the solubilized POH is experiencing rotational hindrance in the clefts due to interactions with the exposed hydrocarbon chains.

Results of PO^- reprotonation are also consistent with the time-dependent penetration of the probe into the bilayer of nonpolymerized **1** vesicles and with its location in the aqueous clefts in polymerized **1** vesicle. After 1 day of incubation, the proton ejection ability of POH is lost in nonpolymerized but unaltered in polymerized vesicles (Table V).

The conceptualization and detailed kinetics for surfactant vesicle photopolymerization reported previously[16] make possible a computer simulation of the process, the aim of which is to provide a graphical visualization and semiquantitative characterization of the resulting surface inhomogeneity and cleft formation. Such a simulation has been carried out[26] and some of the main conclusions are mentioned here.

The main simulation parameters are the monomer–monomer equilibrium spacing in the unpolymerized vesicle, the polymer bond length, the free radical lifetime, the average chain length, and the total number of free radicals produced (i.e., the extent of the polymerization). Carrying the simulation to completion for vesicles with 10 Å of monomer equilibrium spacing, 7 Å of separation between head groups upon polymerization, and an average chain length of 15 monomers/chain shows that over 45% of the interchain separations in fully polymerized vesicles are greater than the equilibrium separation. Furthermore, 50% of these latter interchain separations are greater than 13 Å. Although the openings, or clefts, formed in the vesicle surface can in no way be considered as circular, the value of 13 Å nevertheless provides a rough idea of the linear dimension of the median cleft. The simulation also shows that this median cleft size changes very little with increasing polymerization of the vesicle, and indicates that clefts of this median dimension begin to form as soon as polymerization begins.

Additional kinetic analysis afforded by the simulation shows that, because of free radical trapping and the increasing scarcity of bondable neighbor monomers, the polymer chain lengths decrease in the latter stages of polymerization. The result is that there are many short chains in the final number of chains vs. chain length distribution, although the final weight average distribution of chain lengths is peaked near the kinetically determined average chain length. The overall effect of the chain shortening vs. degree of polymerization is to perturb the weight average chain length distribution from a normal distribution to an asymmetric one in which there is a greater weighting and buildup on the short chain side.

Demonstration of cleft formation upon vesicle surface photopolymerization opens the door to important applications. Suitable compounds may be entrapped and released upon command (depolymerization). Additionally, uniformly sized clefts with restricted polarities may well provide unique sites for reactivity control and molecular recognition.

Acknowledgment. Support of this work by the National Science Foundation and the U.S. Army Research Office is gratefully acknowledged. We thank CNPq Brazil for awards (to F. Nome and M. Politi) and NATO for a travel grant (to P. Tundo).

Registry No. 1, 93253-93-1; POH, 57206-23-2.

Interactions between Phenol and Carbon Monoxide under Cryogenic Conditions. Evidence for a Phenol–CO Complex

J. Gebicki[†] and A. Krantz*[‡]

Contribution from the Department of Chemistry, State University of New York, Stony Brook, New York 11794. *Received June 4, 1984*

Abstract: Phenol has been matrix-isolated in argon, nitrogen, and carbon monoxide. The magnitude of the shifts of key OH bands from gas-phase values indicates that phenol–matrix interactions increase in the series Ar < N_2 < CO. Phenol forms a 1:1 complex with CO in argon-doped matrices. On the basis of the downward shift of ν_{OH} (the OH stretch) and the shift of $\nu_{C\equiv O}$ to higher frequency, it is concluded that phenol is hydrogen bonded to the carbon terminal of carbon monoxide. Phenol in solid carbon monoxide behaves as if there is an equilibrium between "free" and complexed forms. The observation of a 1:1 complex between phenol and CO in argon offers the novel prospect of assessing substituent effects under cryogenic conditions.

Introduction

Complexes formed between proton donors and acceptors have been of essential interest because of their importance to an understanding of intermolecular interactions in biological and chemical systems, and to a general theory of hydrogen bonding.[1-5] The study of one extreme, involving weakly interacting donor and acceptor components of a dimer, is a contemporary activity of

[†] On leave from the Institute of Applied Radiation Chemistry, Technical University, Lodz, Poland, 1979–1981.

[‡] Present address: Syntex, Inc., 2100 Syntex Ct., Mississauga, Ontario, Canada L5N 3X4.

(1) Coulson, C. A. *Research 10* 1957, *149*.
(2) Joesten, M. D.; Schaad, L. J. "Hydrogen Bonding"; Marcel Dekker: New York, 1974.
(3) Pimentel, G. C.; McClellan, A. L. "The Hydrogen Bond"; W. H. Freeman, San Francisco, 1960.
(4) Vinogradov, S. N.; Linnell, R. H. "Hydrogen Bonding"; Van Nostrand-Reinhold: New York, 1971.

0002-7863/84/1506-8093$01.50/0